International Journal of Energy Horizon 01 (2025) 11-19

International Journal of Energy Horizon

journal homepage: https://dergipark.org.tr/tr/pub/ijeh

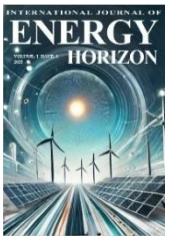

Research Paper

Effect of Metal Foam Material Type and Porosity Pattern on Melting and Flow Dynamics in A Vertical Rectangular Cavity

Emrehan GÜRSOY[1,*]

[1]Audit Department, Kardemir Karabük Iron Steel Industry Trade & Co. Inc., Karabük, Türkiye
[1]ORCID No:0000-0003-2373-3357

ARTICLE INFO

Article History:

Received:13 June 2025
Revised: 17 June 2025
Accepted: 23 June 2025
Available online: 30 June 2025

Keywords:

Different metal foam
Heat transfer enhancement
Latent heat thermal energy storage
Melting
Phase change material

ABSTRACT

Phase change materials have an important role in the field of energy storage. However, due to their low thermal conductivity, transferring applied heat to the entire system is difficult. It negatively affects the lack of use of the systems. Researchers are investigating many applications to prevent this and increase the thermal conductivity of the system. One of these methods is the application of metal foam (MF) embedded inside the phase change material (PCM) in the system. This study investigated the melting and natural convection characteristics of a 2D-designed rectangular cavity, and copper and aluminium MFs were placed inside this cavity, which was separated into two equal compartments. The porosity of these MFs was ε=0.90 and 0.95, and their proximity to the heat source was examined. The Brinkman-Forchheimer extended Darcy model was used in the cases solved based on the finite volume and enthalpy-porosity method. The results showed that RC4 is the case that shows the fastest melting performance, and the solid-liquid interface is not affected by natural convection. Increasing the porosity from ε=0.90 to 0.95 caused natural convection to occur. In these parameters, natural convection increases the thermal resistance and makes it difficult to transfer heat to unmelted phase change materials. It was determined that RC1 is the case that shows the fastest melting after RC4. The melting times of RC4 in Section 1 (S1) and Section 2 (S2) are 2.5 and 1.4 times faster than RC1, respectively. Besides, the placement of MF and porosity significantly affected the Nusselt number (Nu). The average Nu of RC4 is higher than that of RC1, and RC5 at the rate of 34.4% and 48.4%, respectively. As melting progressed, a stationary region was formed in the center of the cavity due to melted PCM moving upward from the hot wall to the cold section.

1. INTRODUCTION

Renewable energy sources, such as solar, wind, hydroelectric, etc., offer high amounts of usable energy, and the amount of instantaneous energy provided by solar is especially much higher than the current human usage needs **[1]**. However, the sustainability of these sources is very limited because of daily, seasonal, and yearly changes **[2]**. Considering these limitations and the ecological impacts of non-renewable energy sources, it is necessary to take action to store energy from a high-capacity source. Energy storage collects energy when it is in excess and makes it available when demand is high **[3]**. Energy can be stored with the help of several methods: thermal, mechanical, chemical, magnetic, and electric **[4]**. Each of these methods is a remarkable method, and the leading method among them is thermal energy storage (TES). TES systems are engineered to store thermal energy through heating, cooling, melting, condensation, or vaporization of a material. Based on the temperature range of operation, these materials are maintained at elevated or reduced temperatures within an insulated container. The stored energy is then retrieved for various purposes, including residential and industrial applications such as space heating or cooling, hot water generation, or power production.

Thermal energy can be stored in many ways and this classification has been presented by **[5]**. As stated in their study, sensible, latent, and thermo-chemical methods carry out the storage process in TES. Among these methods, the latent heat thermal energy storage (LHTES) method uses phase change material (PCM). This material has become the focus of more research and interest compared to other methods due to its advantages, such as high heat storage capacity, isothermal behaviour during melting and freezing processes, and minimum system size **[6, 7]**.

Although PCM has significant advantages, there are also serious disadvantages to its use in thermal systems, such as low thermal conductivity. However, it has been proven by many researchers using experimental and numerical analyses that this disadvantage can be improved by making enhancement applications, including metal foams (MFs), nanoparticles, magnetic fields, etc., on the systems, and some of these studies in renewable energy systems are numerically investigated an innovative 3D photovoltaic thermal (PVT) system integrated with PCM and MF **[8]**. By introducing copper (Cu) MF with varying porosities (ε) within the PCM compartment and employing nanofluid as the working fluid, the research evaluates the effects of parameters such as mass flow rate, nanofluid concentration, and ε on thermal and electrical performance.

*Corresponding author
E-mail address: emrehangursoy@gmail.com
journal homepage: https://dergipark.org.tr/tr/pub/ijeh

Results indicate that increasing ε from 0.2 to 0.8 enhances thermal efficiency by 33%, with a slight electrical efficiency decrease of 2.6%. Additionally, the PVT/PCM+Cu MF system achieves a 25.4% higher thermal efficiency compared to the PVT/PCM configuration, underscoring the effectiveness of incorporating Cu MF. To enhance the melting rate of MF composite PCM, partial and gradient optimizations of the MF pore densities (ω) were explored by Li et al. **[9]**. Among the partially optimized models, Partial-80-5-5 exhibited the most efficient melting, highlighting that increasing ω in the top region significantly accelerates the melting process. Further analysis of models with varying top-region ω confirmed that higher densities lead to faster melting. Gradient optimizations, such as Gradient-80-40-5, achieved the fastest melting rate overall. This performance is attributed to strong vortex formation at the bottom region, induced by suppressed natural convection in the top and middle regions with high ω. Ami Ahmadi et al. explored using gradient MFs with graded ε to improve TES performance.

Numerical simulations of a shell-and-tube TES unit showed that arranging MFs with ε ranging from 0.65 to 0.94 in the PCM domain reduces charging time and entropy generation **[10]**. Optimized designs achieved a 3.35% faster charging time and 7.96% lower entropy generation compared to uniform ε, demonstrating the effectiveness of gradient MFs. Prasanth et al. focused on enhancing the thermal conductivity of PCMs for solar thermal energy storage using Cu MF and Cu/aluminium (Al) wire-woven MF structures **[11]**. LHTES systems with a 300 KJ capacity were designed. Both PCM-Al wire woven MF and PCM-Cu MF composites exhibited similar melting times, but the heat extraction performance of the Al wire woven MF was comparable to Cu MF. Thermal efficiency ranged from 60–70% with water and 80–85% with air as heat extraction media. Heat extraction lasted 3–4 hours with cold water and 7–8 hours with cold air, increasing the outlet temperature by 2–2.5 times the inlet temperature. A pore-scale numerical model is developed by Parida et al. to simulate the melting of PCMs in PCM-MF composite energy storage systems **[12]**.

Unlike volume-averaged approaches, this model resolves the MF geometry, enabling accurate analysis of ω, distribution, and localized heat transfer at the PCM-MF interface. Incorporating convection effects, the model uses an enthalpy-based Finite Volume Method (FVM) and is validated against experimental data. Results show that convection significantly enhances melting and energy storage rates, particularly for MFs with higher ε and larger ω. Nie et al. investigated the effect of geometry on the melting and solidification behaviour of PCMs in seven vertical shell-tube LHTES systems **[13].** Both pure PCM (paraffin RT82) and composite PCM (paraffin RT82 embedded in Cu MF) are examined. A two-dimensional numerical model based on the enthalpy-porosity method (EPM) is developed and validated with experimental data. Results show that the conical shell system enhances natural convection, while the frustum tube system improves both convection and conduction. Geometry modification reduces melting time by at least 9.2% for pure PCM and 5.9% for composite PCM. The frustum tube system outperforms the conical shell system in both melting and solidification processes, regardless of the MF or working fluid used. Karimi et al. explored the use of PCMs in LHTES systems for buildings, addressing the issue of low thermal conductivity that limits charge/discharge rates **[14]**.

A new design incorporating a helical coil filled with PCM on both sides and Cu MFs (ε=0.9 and ω=12 PPI) in the inner region is proposed to enhance heat transfer. The effects of parameters such as HTF inlet flow rate, temperature, and MF on thermal performance are analysed experimentally. Results show that MF can reduce charge/discharge time by up to 57%, with greater reductions observed at higher inlet working fluid temperatures. Increasing the working fluid flow rate slightly shortens charging time, especially with MF, and accelerates discharge time, with faster depletion at lower working fluid inlet temperatures. Ghalambaz et al. investigated the effect of MF layer configurations on melting time in a system with parallel channel enclosures **[15]**. Three configurations were tested: half-split, L-shape, and diagonal foam layers. The optimal design was a horizontal split with a light foam layer at the top, which reduced charging time by 32%, completing the process in 837 seconds. Liu et al. examined the use of MF structures with varying ε gradients and multiple PCMs with different melting points to enhance PCM melting and improve system efficiency **[16]**.

Results show that using multiple PCMs reduced melting time by 9.18% compared to a single PCM with uniform MF. A multi-PCM system with ε=0.90 was tested with one-dimensional and two-dimensional porosity gradients. The one-dimensional positive gradient reduced melting time by 6.18%, while the negative gradient increased it by 19.78%, though the negative gradient minimized temperature non-uniformity. The optimal two-dimensional gradient model reduced melting time by 17.96% and increased energy storage efficiency by 20.16% compared to the single PCM system with uniform ε. A dimensionless analysis was also conducted to model liquid fraction (β) about Fourier, Stefan, and Rayleigh numbers. Joshi and Rathod, compared the thermal performance of fins and MF infusion in LHTES systems with identical compactness factors **[17]**. An experimental test rig validated a numerical model based on the coupled EPM. Results show that fins enhance thermal transport by 50% during melting and 5.56% during solidification compared to pure PCM. MF infusion improves thermal transport by 16.67% during melting and 33.33% during solidification. Fins accelerate melting by 66.67%, but MF enhances solidification by 29.41%. Overall, MF reduces total cycle time by 15%, making it a more effective thermal performance enhancer than fins. This numerical study conducted by Haddad et al. optimized the melting performance of TES partially filled with MF **[18]**.

A FVM based on the EPM was used for simulations, exploring the effects of foam location, ε, and nanoparticle volume fraction. The results show that inserting the MF layer diagonally from the top left to right bottom minimizes melting time. Compared to pure PCM, the melting time increases by 77.7%, while stored energy decreases by 6.7%. The optimal ε is 0.88, offering nearly the same stored energy as pure PCM with a 4% deviation. Adding nanoparticles enhances the melting rate by 8% but reduces stored energy by 3%. Hybrid systems combining MF at optimal ε and nanoparticles are more efficient than using each technique separately. Mehryan et al. investigated the melting heat transfer of capric acid PCM in a TES, using Cu nanoparticles and Cu MF to improve charging time **[19]**.

The EPM, combined with the FVM, simulates the free convection melting heat transfer of composite PCM. The ε, shape of the Cu MF layer, and nanoparticle volume fraction were optimized using the Taguchi approach to minimize charging time. Results showed that a left-right triangle porous zone minimized charging time. Higher ε and nanoparticle volume fraction further reduced charging time. The optimal combination of Cu MF, Cu nanoparticles, and MF design reduced melting time by three times, with a 12.8% and 21.96% reduction in charging time for MF zone configurations. Chibani et al. investigated the melting process of PCM embedded with nanoparticles and MF in a shell-and-tube LHTES, using numerical simulations **[20]**.

The model was first validated with experimental data. The effects of adding 5% Al_2O_3 nanoparticles and using various MFs (Al, Cu, Nickel, Titanium) with ε ranging from 0.96 to 0.99 were compared regarding temperature and liquid fraction during melting. The MF-PCM systems outperformed pure and nano-enhanced PCM, significantly reducing melting time. The effectiveness of the MFs followed the thermal conductivity order: Cu>Al>Ni>Ti. Increasing ε reduced melting time, with the highest porosity (ε=0.99) yielding the best performance. This study optimizes the design for improved practical application and reduced energy waste.

When the literature is examined, many methods and configurations have been used and examined to increase the thermal conductivity of PCM used for heat storage. However, due to these examinations, melting performance and natural convection characteristics of a LHTES including MF manufactured from two different materials with different physical property variables according to the heat source have not been examined in detail. In this study, one-half of a rectangular LHTES volume was filled with Al MF and Cu MF with ε=0.9 and 20. The entire volume of the rectangular LHTES was filled with RT-58 PCM material and heated from a single wall. In the numerical analyses where the MF in contact with the hot wall was also variable, a total of 6 different configurations were analysed.

2. DESCRIPTION OF MODEL AND MATHEMATICAL BACKGROUND

A schematic view of rectangular LHTESs is presented in Figure 1. Entire geometric, morphologic, and boundary conditions are similar to each system. A rectangular cavity was formed considering 30 cm height and 10 cm width. 350K has been applied to the left wall of the cavity, and the other wall is considered adiabatic. Moreover, the no-slip condition was applied to all walls. Also, the geometry was divided into two equal parts, and half volumes were filled with Al and Cu MFs, which changed the arrangement based on the thermal wall. MF parameters ε and ω were selected as 0.9 and 20 PPI, respectively, after the detailed investigation of the literature based on the Refs **[21-23]**. Variants of these structural parameters, as well as the arrangement of MFs, were used. Because of this, six different cases including the parameters in Table 1 have been analysed.

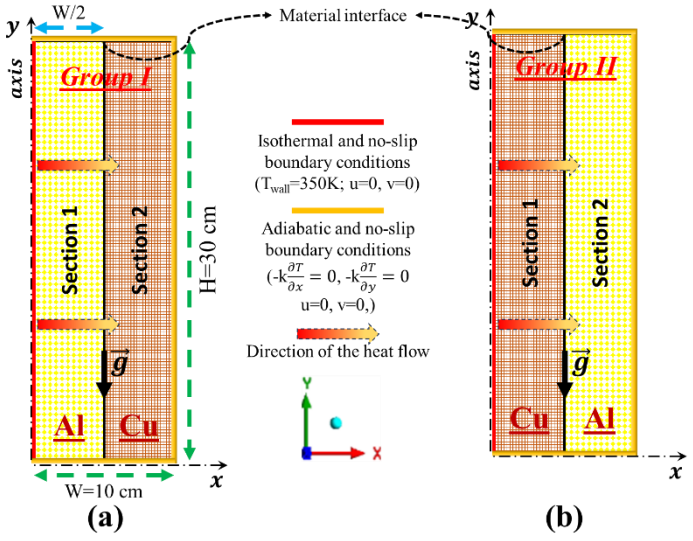

Figure 1. Schematic view of the computational domains for; (a) Group I (Al contacts hot wall) and (b) Group II (Cu contacts hot wall).

Table 1. Physical configuration of computational domains

Group I						
Case No	Section 1			Section 2		
	Material	ε	ω	Material	ε	ω
RC1	Al	0.9	20	Cu	0.9	20
RC2	Al	0.95	20	Cu	0.9	20
RC3	Al	0.95	20	Cu	0.95	20
Group II						
Case No	Section 1			Section 2		
	Material	ε	ω	Material	ε	ω
RC4	Cu	0.9	20	Al	0.9	20
RC5	Cu	0.95	20	Al	0.9	20
RC6	Cu	0.95	20	Al	0.95	20

The mentioned above cases have been solved based on the FVM combined with EPM **[24]**. The Brinkman-Forchheimer extended Darcy model **[25]**, and the local thermal equilibrium (LTE) hypothesis was used to characterize the MF in the analyses **[26]**. The continuity, momentum, and energy (for LTE) governing equations used in melting process solving are given in Eq. 1-3 **[27]**, respectively. While applying these equations, some assumptions are given below, taking into account.

- The analysis is carried out for a two-dimensional axisymmetric geometry.
- Due to the low-temperature difference between the solidus and liquidus temperature of PCM, the Boussinesq approximation has been used for calculating the density **[28]**.
- Thermophysical properties of PCM and MFs are considered constant.
- In the energy equation, the effect of viscosity is neglected.
- Computational domain volume is not changed during the melting process.
- Structural modification of MFs is accepted as isotropic and homogeneous.

$$\nabla \cdot V = 0 \tag{1}$$

where, V [m.s^{-1}] shows the PCM velocity in the rectangular cavity.

$$\frac{\rho_p}{\varepsilon}\frac{\partial V}{\partial t} + \frac{\rho_p}{\varepsilon^2} V \cdot \nabla V = -\nabla p + \frac{\mu_p}{\varepsilon}\nabla^2 V - \frac{(1-\beta)^2}{(\beta^3+0.001)} A_{mush} V - \left(\frac{\mu_p}{K} V + \frac{C_F}{\sqrt{K}}\rho_p V|V|\right) + \rho_p g \gamma \Delta T_0 \tag{2}$$

in which, g [m.s^{-2}], ρ [kg.m^{-3}], p [Pa], T [K], A_{mush} [kg.m^{-3}.s^{-1}], K [m^2], and C_F [m^{-1}] symbolize the gravity (g=9.91 [m.s^{-2}]), density, pressure, temperature, mush zone constant (set to 10^5 kg.m^{-3}.s^{-1}), permeability, and Forchheimer's drag coefficient (inertial).

$$(\rho c_p)_{eff}\left(\frac{\partial T}{\partial t} + V \cdot \nabla T\right) = k_{eff}\nabla^2 T - \varepsilon \rho_p H_L \frac{\partial \beta}{\partial t} \tag{3}$$

where, c_p [J.kg^{-1}.K^{-1}], k [W.m^{-1}.K^{-1}], and H_L [kJ.kg^{-1}] describe the specific heat, thermal conductivity, and latent heat energy. Incorporating MF enhances the thermal conductivity of the process named effective and this property is calculated with Eq. (4) **[29]**.

$$k_{eff} = \varepsilon k_{PCM} + (1-\varepsilon) k_{MF} \tag{4}$$

Other characteristic properties calculated based on the given structural properties with ε=0.9 and ω=20 PPI for both MFs are presented in Table 2. Besides, the thermo-physical properties of RT-58 (Rubitherm) PCM, Al MF, and Cu MF have been presented in Table 3.

Table 2. Equations used to calculate MF structural properties **[30]**

Definition	Equation	Eq.
Permeability, [m^2]	$K = \frac{\varepsilon^2 d_k^2}{36(\delta^2 - \delta)}$	(5)
Characteristic length, [m]	$d_k = \frac{\delta}{3-\delta} d_p$	(6)
Tortuosity coefficient	$\delta = 2 + 2\cos\left[\frac{4\pi}{3} + \frac{1}{3}\cos^{-1}(2\varepsilon - 1)\right]$	(7)
Forchheimer's drag (inertial) coefficient, [1/m]	$C_F = 0.00212(1-\varepsilon)^{-0.132}\left(\frac{d_f}{d_p}\right)^{-1.63}$	(8)
Fiber diameter, [m]	$d_f = 1.18\sqrt{\frac{1-\varepsilon}{3\pi}}\left(\frac{1}{1-e^{\left(-\frac{1-\varepsilon}{0.04}\right)}}\right)$	(9)
Pore diameter, [m]	$d_p = \frac{0.0254}{\omega}$	(10)

Table 3. Thermophysical properties of RT58, Al MF, and Cu MF.

Properties	RT58 **[31]**	Al **[32]**	Cu **[33]**
Density, ρ [kg.m^{-3}]	825	2719	8900
Specific heat, c_p [J.kg^{-1}.K^{-1}]	2000	871	385
Thermal conductivity, k [W.m^{-1}.K^{-1}]	0.2	202.4	401
Dynamic viscosity, μ [kg.m^{-1}.s^{-1}]	0.0269	-	-
Thermal expansion coefficient, γ [K^{-1}]	0.00011	-	-
Latent heat, H_L [J.kg^{-1}]	160000	-	-
Solidus temperature, T_S [K]	326	-	-
Liquidus temperature, T_L [K]	332	-	-

The EPM is applicable for scenarios where melting occurs progressively across a finite temperature range without a well-defined melting front. This method defines three distinct phases during the melting process: a solid phase where β=0, a mixed solid-liquid phase (mushy) where 0<β<1, and a liquid phase where β=1. The value of β depends on the local temperature and is determined using Eq. (11).

$$\beta = \frac{\Delta H}{H_L} = \begin{cases} 0 \text{ if } < T_S \\ \frac{T - T_S}{T_L - T_S} \quad \text{if } T_S < T < T_L \\ 1 \text{ if } T > T_L \end{cases} \tag{11}$$

where, T_S [K], T [K], and T_L [K] represent the temperatures of the solid phase, the local region, and the liquid phase, respectively. The region with a temperature below T_S is entirely solid, whereas the area with a temperature above T_L is fully liquid. Melting occurs when the temperature is within the range between T_S and T_L. In all cases, the initial temperature (T_{in}) is 298.15 K.

The governing equations were solved using ANSYS FLUENT 2024 R1 software considering the boundary and initial conditions of the computational domains and a time-dependent FVM analysis was carried out. To provide a sustainability pressure field, the SIMPLE algorithm was selected, and PRESTO! scheme was employed for pressure calculations. Besides, the second-order upwind scheme method was preferred to calculate the momentum and energy equations while residual trends were set to 10^{-6}.

After determining the physical properties and mathematical background, mesh convergence and time step size sensitivity analyses required for time-dependent numerical analyses should be performed to provide highly reliable results. In this context, the mesh convergence analysis of the rectangular LHTES in question was conducted for mesh numbers 3465, 7500, and 13333, and the time step sensitivity analysis was conducted for t=0.1, 0.5, and 1.0s, and the obtained liquid fraction-time graphs are presented in Figure 2(a) and Figure 2(b), respectively. When investigating the trends, it can be said that mesh number and time step size did not affect the results. According to the numerical results, the average deviation of 0.51% and 0.74% are calculated between 3465-13333 and 7500-13333, respectively, considering the mesh number at *t*=0.5s. On the other side, 0.71% and 0.83% average deviations were detected between *t*=0.1-0.5s and *t*=0.1-1.0s for time step size sensitivity analysis, respectively, at 7500 mesh number. Based on these results, a mesh number of 7500 and a time step size of *t*=0.5s have been selected to solve further solutions. On the other hand, the mesh structure of the computational domain is given in Figure 3.

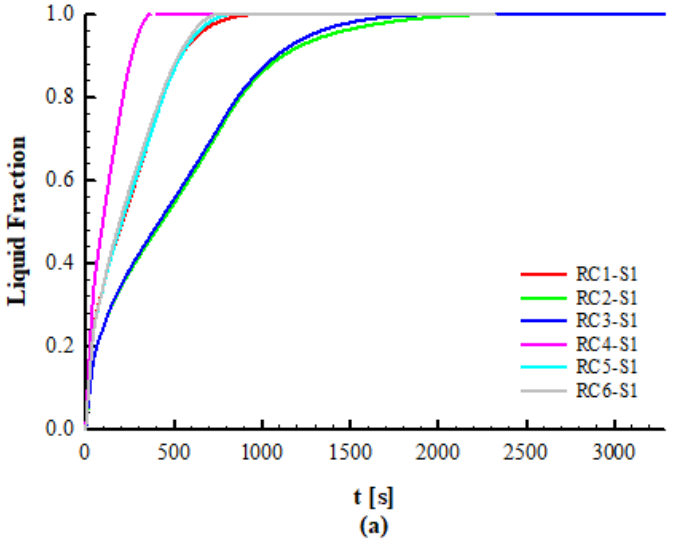

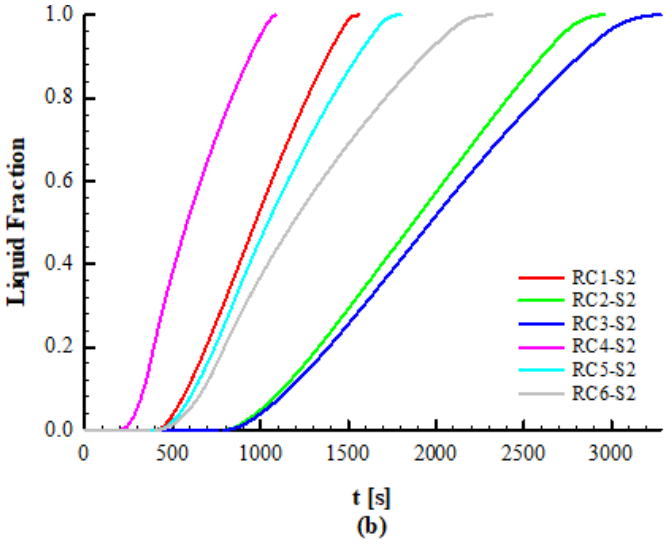

Figure 2. Imperative analyses before major solutions; (a) mesh convergence analysis at t=0.5s and (b) time step size sensitivity analysis at 7500 mesh number.

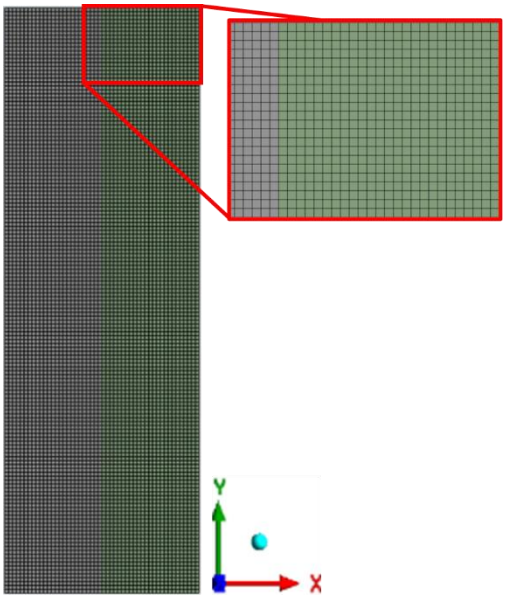

Figure 3. The mesh structure belongs to the 7500 mesh number.

Before proceeding to the analyses where the final results will be obtained, the solution methods and mesh structure of the numerical analysis, that is, the entire analysis setup, must be validated. In this context, the necessary validation is compared with the liquid fraction function of the study conducted by Huang et al. both as a contour and graphically in Table 4 and Figure 4, respectively **[30]**. When the contours are examined, it is concluded that the liquid-solid interface has almost the same distribution at all t times. When the numerical values in the trends are examined, it is calculated that the average deviation value between the two trends is 0.81%. With these results, it can be concluded that all solution procedures and applications applied in the study provide results compatible with the literature.

Table 4. Validation of the results as a liquid fraction contour.

t [s]	60	180	360	540	720	900
Huang et al. **[30]**	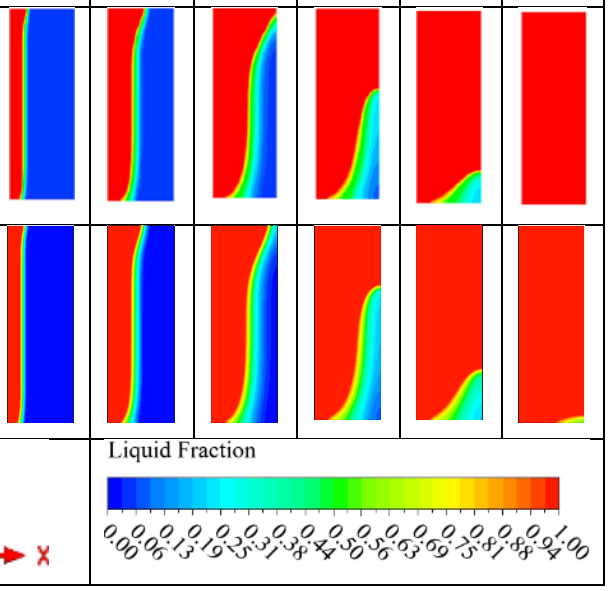					
Present study						

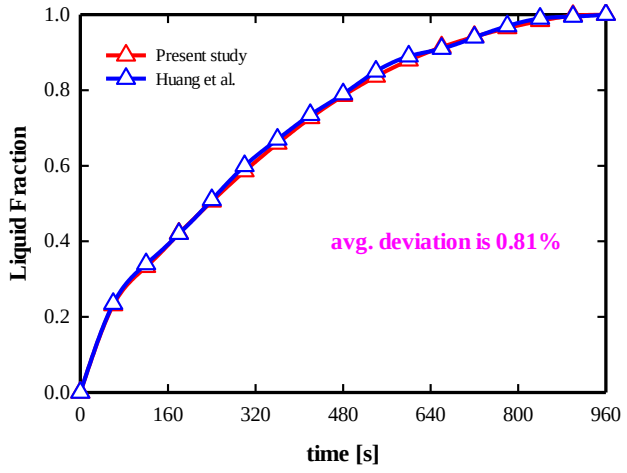

Figure 4. Validation of the results with Huang et al. study as a liquid fraction trend **[30]**

3. RESULTS AND DISCUSSION

The liquid fraction performance of the cases is examined in Figure 5. When Figure 5(a) showing the S1 characteristic is examined, the RC4, RC5, and RC6 cases, where the hot wall is in contact with the Cu MF, give the fastest response to the heating effect. The main reason for this situation is the increase in effective thermal conductivity in the cases due to the higher thermal conductivity of Cu MF. According to the results, RC4 reached full melting at the earliest time (t=1120 s). At t=1120 s, the melting rates of PCM in RC1, RC2, RC3, RC5 and RC6 are controlled at 82.9%, 49.9%, 49.7%, 78.5% and 72.8%, respectively. It can also be understood that the porosity of Cu MF, ε=0.95, exhibits a similar characteristic with the ε =0.9 of Al MF, which is close to the wall. From this result, it is undeniable that in addition to considering how high the thermal conductivity of the MF material used is, its porosity should also be taken into account. In S2, the fastest performance was again shown by RC4 in Figure 5(b), although Al MF was. The factor that caused this situation is that Cu MF, positioned on the hot wall with a low porosity, can conduct heat at a good level and Al MF with ε=0.9 can also respond quickly to this performance. However, as the porosity of Cu MF in S1 increases, RC4 shifted to another characteristic mechanism mentioned above and the second fastest performance in S2 was realized in RC1. This is the decrease in the level of heat conduction due to the decreasing amount of conductive material per unit volume as the porosity increases. A similar result has been found by Ami Ahmadi et al. **[10]**. Since the low porosity value contains more MF with high conductivity in volume, in these cases the heat transfer mechanism in the system is mostly carried out by conduction. In cases consisting of high porosity MF, an environment is created in the system where the PCM can move more easily and natural convection increases. However, thermal resistance also tends to increase at this point.

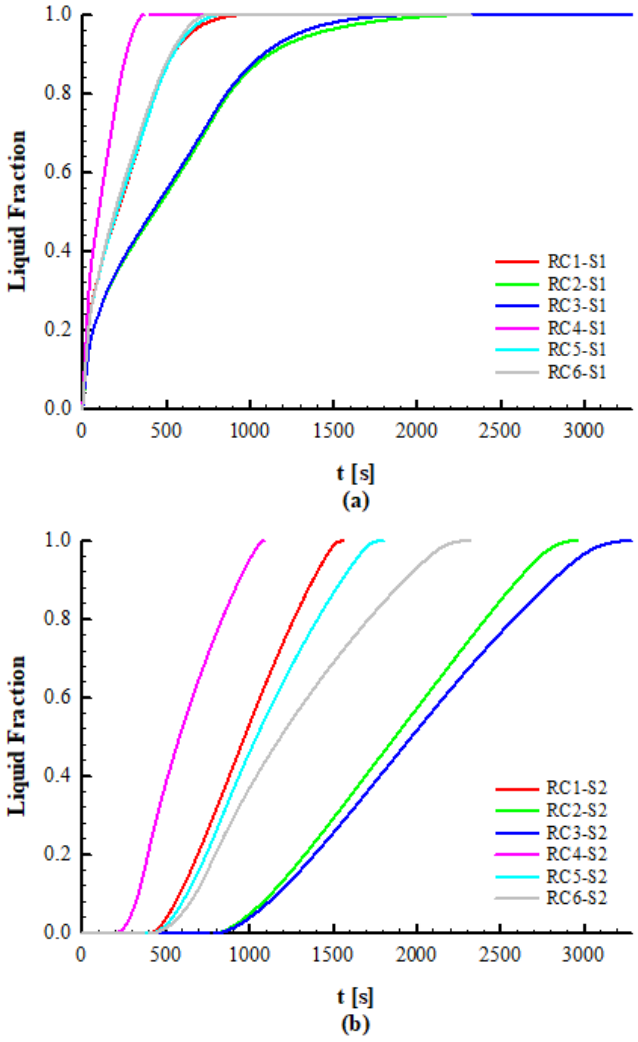

Figure 5. Liquid fraction characteristics in; (a) S 1 and (b) S2 as a function of time.

The liquid fraction behaviour of the cases is presented as contour in Table 5. Along with these contours, solid-liquid interfaces can be seen and the heat transfer progress in LHTES can be understood. When the figures are examined, it is observed that the solid-liquid interface in RC4 progresses faster and melts earlier. In this melting process, it is seen that the solid-liquid interface, which is in contact with the lower and upper points of the rectangular cavity, is in the form of a vertical line throughout the melting process. The main factor causing this situation is that the porosity of the MFs placed in the sections in RC4 is ε= 0.9. This parameter occupies more volumetrically the conductive material forming the MF and does not allow natural convection, and the heat transfer from the hot wall occurs by conduction throughout the process.

On the other hand, the thermal conductivity of the material from which the MF is manufactured is as important as the porosity of the MF. Although there is Cu MF with a porosity of ε= 0.95 in S1 of RC5 and RC6, no considerable tendency towards natural convection is observed here. However, when the heat reached S2, which consists of Al MF, the solid-liquid interface showed a logarithmic trend in the upper region of the rectangular cavity due to the decrease in the density of the PCM melted in the lower region of the rectangular cavity and the effect of the buoyancy force. The reason for this situation is that the porosity of S1 in RC5 is ε=0.95 and therefore the PCM finds more space to move in the cavity. In RC6, the porosity is ε=0.95 for both Sections and it is observed that the solid-liquid interface becomes more pronounced.

From these results, it can be determined by the behavior of the solid-liquid interface that the parameters of the MF material and porosity in the rectangular cavity directly affect the complete melting process of LHTES.

Figure 6 depicts the final melting time of the sections. According to the results, RC4 reaches the fully melted state first because in this case, the MF near the hot wall is Cu MF with high thermal conductivity and the porosity in both sections is ε=0.90. The combination of these two phenomena makes RC4 the fastest fully melted state. On the other hand, the case that provides the second fastest melting performance is RC1. Although Al MF is placed in the section close to the hot wall, the porosity being ε=0.9 in all sections made RC1 melt faster than the other cases. From these results, it can be inferred that the porosity is more important than the material type of the MF integrated into the system. The complete melting time in the S1 and S2 regions of RC4 was 2.5 and 1.4 times faster than that of RC1, respectively.

Table 5. Comparison of liquid fraction contours of the cases as a function of the time

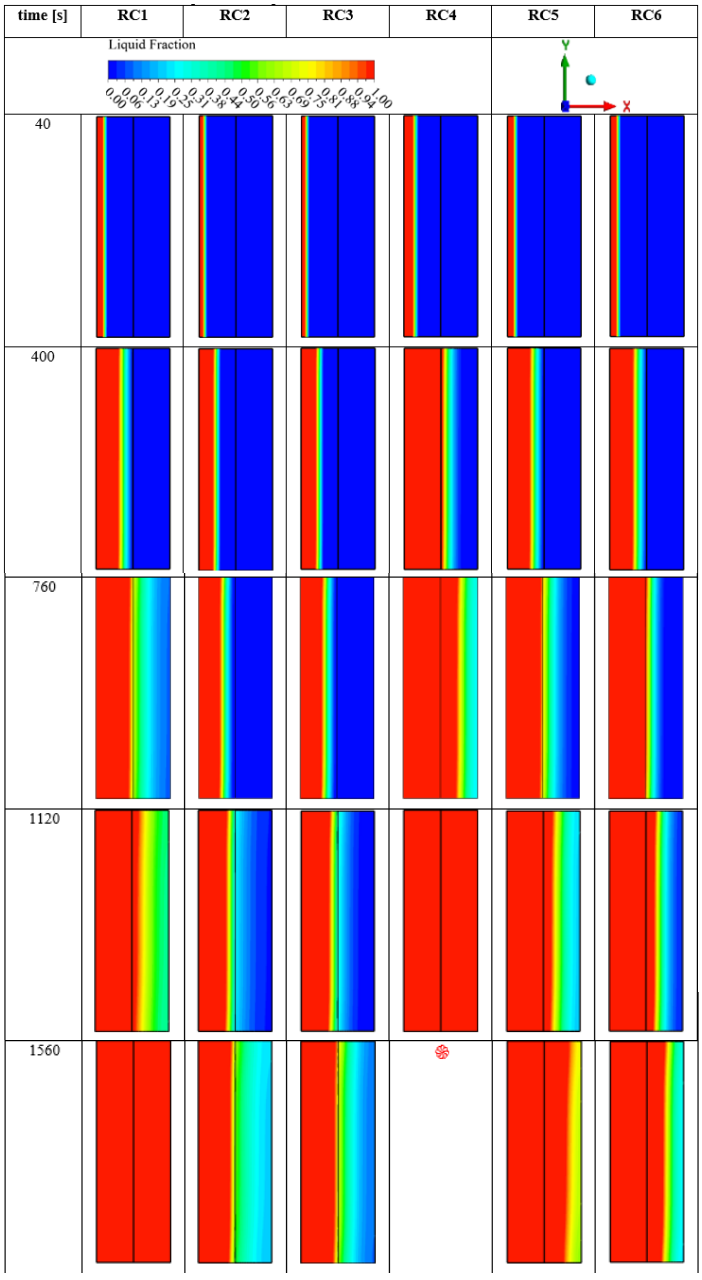

Figure 6 depicts the final melting time of the sections. According to the results, RC4 reaches the fully melted state first because in this case, the MF near the hot wall is Cu MF with high thermal conductivity and the porosity in both sections is ε=0.90. The combination of these two phenomena makes RC4 the fastest fully melted state. On the other hand, the case that provides the second fastest melting performance is RC1. Although Al MF is placed in the section close to the hot wall, the porosity being ε=0.9 in all sections made RC1 melt faster than the other cases. From these results, it can be inferred that the porosity is more important than the material type of the MF integrated into the system. The complete melting time in the S1 and S2 regions of RC4 was 2.5 and 1.4 times faster than that of RC1, respectively.

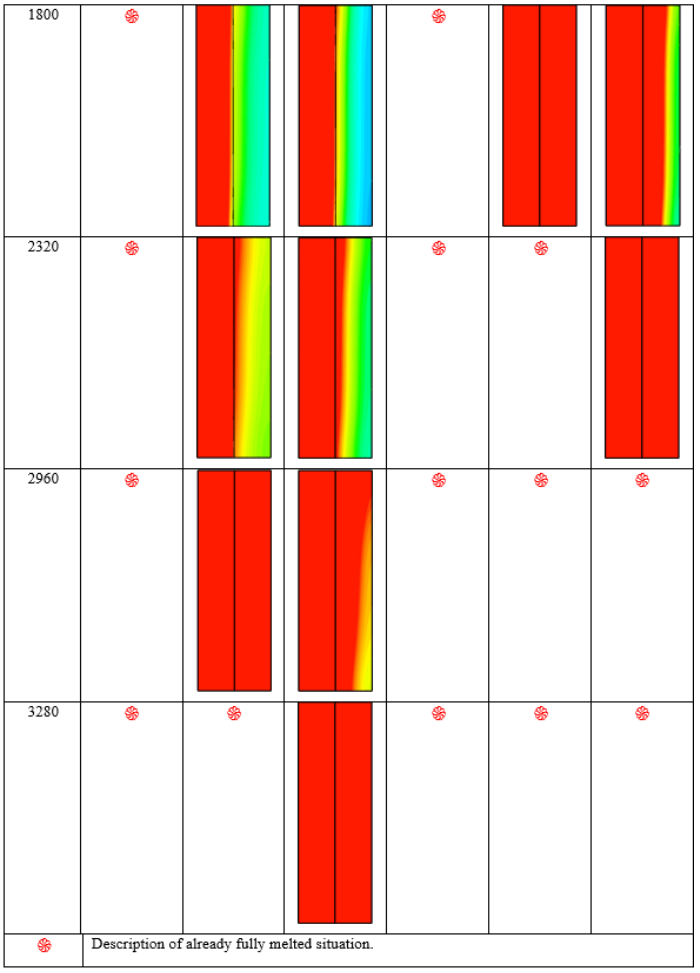

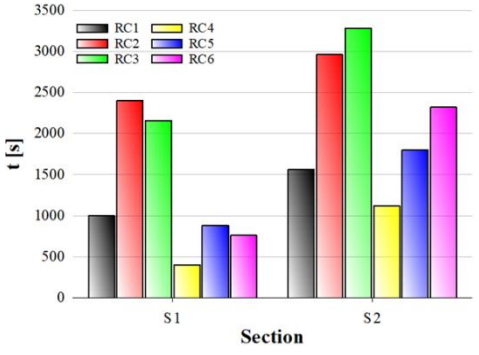

Figure 6. Full melting time performance of the cases

To evaluate the effectiveness of heat transfer throughout the melting process, the time-dependent Nusselt number (Nu) variation is given in Figure 7. At the onset of melting, Nu shows a sudden increase due to heat transfer predominantly realized by conduction.

The results show that placement and porosity of MFs important for the progress of the heat and the cases of Cu MF near the hot wall performed the highest Nu compared to identical configurations. The average Nu of RC4, RC5, and RC6 is 34.4%, 59.6%, and 35.5% higher than that of RC1, RC2, and RC3, respectively. On the other hand, increasing porosity also negatively affects the heat progression in the LHTES, and the change in S1 affects this progression more than the change in S2. This can be obtained by comparing the changes in average Nu between RC4-RC5 and RC5-RC6. RC4 with a porosity of ε=0.90 in S1 transfers 48.4% more heat than RC5 with a porosity of ε=0.95, and RC5 with a porosity of ε=0.90 in S2 transfers 23.3% more heat than RC6 with a porosity of ε=0.95.

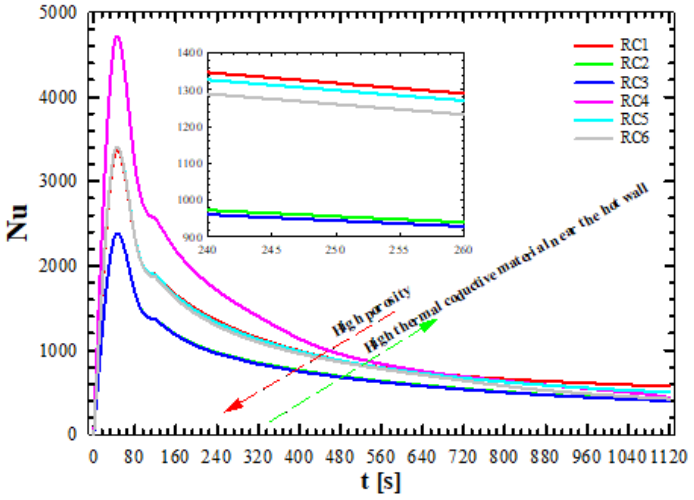

Figure 7. Effect of MF material and porosity configuration on time-dependent Nu

Table 6 illustrates the natural convection flow pattern in the cases up to t=1120 s. Velocity vectors reveal the flow characteristics arising from natural convection and directly affect the convective heat transfer effectiveness. At the beginning of the melting process, in all configurations, the flow field remained quite weak and the velocity magnitudes remained at low levels. This situation shows that PCM substantially remained in a solid form and natural convection did not enhance. As the melting progresses over time, increases in the natural convection intensity were observed due to temperature differences occurring in the liquid phase.

Compared to liquid fraction variation in Table 5, velocity vectors remain limited beyond the melted region, and high-velocity magnitudes were shown as the boundaries. A stationary area was formed in the central region of the cavity by the formation of a typical natural convection cycle (from left to right) characterized by the upward movement of the hot liquid and the downward movement of the cold liquid. These high velocities disappear with the complete melting of the PCM, and it is obvious that the changes in the velocity vectors between the cases are directly shaped according to the alignment and thermal conductivity of the MF.

Table 6. Comparison of velocity vectors of the cases as a function of the time

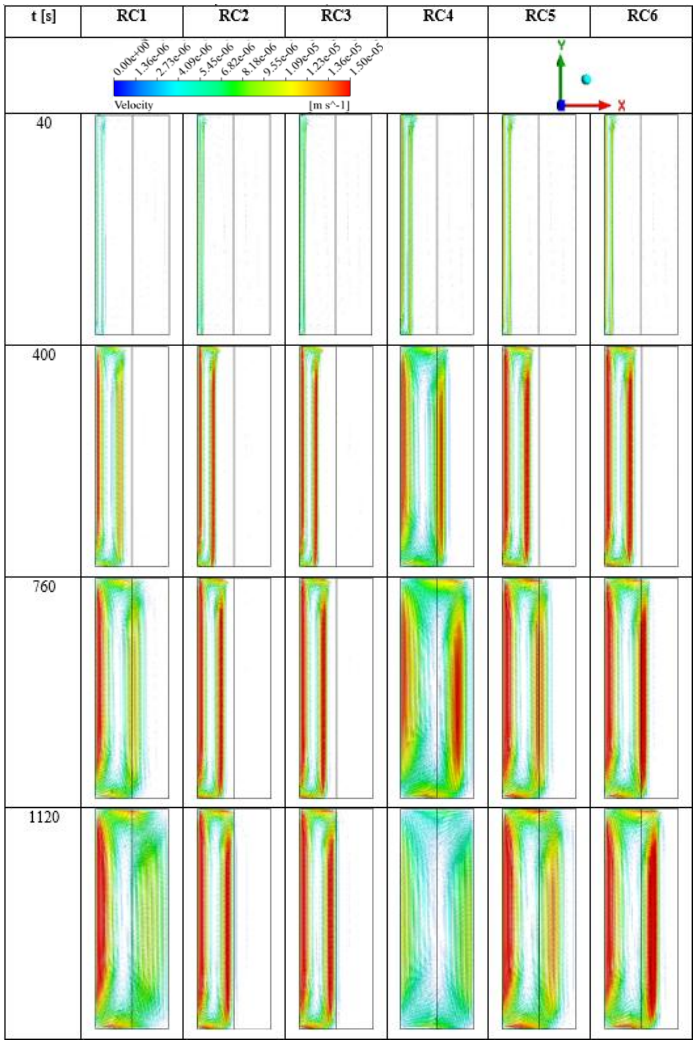

4. CONCLUSION

This paper includes the investigation of different MF types and configurations on melting dynamics and flow characteristics of rectangular LHTES. In the study, a 2D numerical model was developed and six different case configurations were solved based on EPM and the Brinkman-Forchheimer extended Darcy model. Dynamic responses of melting performance and natural convection characteristics have been presented and compared with each other. According to this purpose, the major findings are listed as follows:

1) Cu MF, where placed in S1, quickly responded to the heating effect due to it having higher thermal conductivity.

2) The RC4 case performed the highest melting process because the solid-liquid interface progressed faster.

3) In the RC4 case, the solid-liquid interface contacted with the lower and upper points of the rectangular cavity shows vertical progress. The main reason for this situation is related to low porosity in both sections, and Cu MF is the material conducting the heat into the further section.

4) When S1 was filled with Cu MF with ε=0.95 and S2 with Al MF, the solid-liquid interface showed a logarithmic trend in the upper region of the rectangular cavity; this is due to the decrease in the density of molten PCM in the lower region of the rectangular cavity and the effect of buoyancy force.

5) The second faster melting performance has been observed in RC1. This result shows that porosity is more important than the material type of the MF and that the full melting time in the S1 and S2 regions of RC4 was 2.5 and 1.4 times faster than that of RC1, respectively.

6) The placement of MF with higher thermal conductivity on the hot wall and lower porosity contributed to the improvement of heat transfer in LHTES. RC4 has a 34.4% higher Nu performance than RC1 and 48.4% higher Nu performance than RC5.

7) A stationary region was formed in the center of the cavity due to melted PCM moving upward from the hot wall to the cold section due to buoyancy force as melting progresses. Besides, the velocity in the LHTES significantly relies on the alignment and thermal conductivity of the MF.

5. FUTURE PERSPECTIVE

In future studies, the effects of different types of MF materials, porosity levels, and geometric arrangements with PCMs on heat transfer can be investigated more comprehensively. In addition, the effects of composite structures formed by adding nanoparticles to MF on thermal performance can be investigated, and hybrid improvement methods can be evaluated. In addition, magnetohydrodynamic studies can be conducted if the nanoparticles are magnetic. Experimental verification studies conducted under variable thermal boundary conditions reflecting real operating conditions will increase the validity of the numerical results obtained. In this context, application-based research supported by energy and exergy analyses will make significant contributions to the design of more efficient and sustainable thermal energy storage systems.

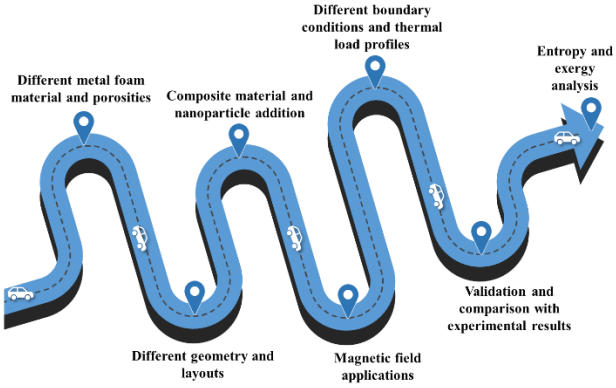

Figure 8. Schematic illustration of the proposed roadmap for future studies focusing on the enhancement of thermal performance in LHTES systems using metal foam-PCM composites.

Nomenclature			
A_{mush}	mush zone constant, [$kg.m^{-3}.s^{-1}$]	T	temperature [K]
c_p	specific heat, [$J.kg^{-1}.K^{-1}$]	TES	thermal energy storage
C_F	Forchheimer' s drag (inertial) coefficient, [m^{-1}]	V	velocity [$m.s^{-1}$]
d_f	fiber diameter, [m]	Greek symbols	
d_k	characteristic length, [m]	β	liquid fraction
d_p	pore diameter, [m]	ω	pore density, [PPI]
EPM	enthalpy-porosity method	ε	porosity
FVM	finite volume method	ρ	density, [$kg.m^{-3}$]
g	gravity, [$m.s^{-2}$]	δ	tortuosity coefficient
H_L	latent heat, [$J.kg^{-1}$]	∀	unit volume [m^3]
k	thermal conductivity, [$W.m^{-1}.K^{-1}$]	μ	dynamic viscosity, [$kg.m^{-1}.s^{-1}$]
K	permeability [m^2]	γ	thermal expansion coefficient, [K^{-1}]
LHTES	latent heat thermal energy storage	Subscripts	
MF	metal foam	in	initial
p	pressure, [Pa]	L	liquidus
PCM	phase change material	S	solidus
S	section		

REFERENCES

[1] A. Rahman, O. Farrok, and M. M. Haque, "Environmental impact of renewable energy source based electrical power plants: Solar, wind, hydroelectric, biomass, geothermal, tidal, ocean, and osmotic," *Renewable and Sustainable Energy Reviews*, vol. 161, Art. no. 112279, 2022, doi: 10.1016/j.rser.2022.112279.

[2] A. Razmjoo, L. G. Kaigutha, M. A. Vaziri Rad, M. Marzband, A. Davarpanah, and M. Denai, "A technical analysis investigating energy sustainability utilizing reliable renewable energy sources to reduce CO_2 emissions in a high-potential area," *Renewable Energy*, vol. 164, pp. 46–57, 2021, doi: 10.1016/j.renene.2020.09.042.

[3] G. Sadeghi, "Energy storage on demand: Thermal energy storage development, materials, design, and integration challenges," *Energy Storage Materials*, vol. 46, pp. 192–222, 2022, doi: 10.1016/j.ensm.2022.01.017.

[4] J. Mitali, S. Dhinakaran, and A. A. Mohamad, "Energy storage systems: a review," *Energy Storage and Saving*, vol. 1, no. 3, pp. 166–216, 2022, doi: 10.1016/j.enss.2022.07.002.

[5] I. Sarbu and C. Sebarchievici, "A comprehensive review of thermal energy storage," *Sustainability*, vol. 10, no. 1, Art. no. 191, 2018, doi: 10.3390/su10010191.

[6] S. Khare, M. Dell'Amico, C. Knight, and S. McGarry, "Selection of materials for high temperature latent heat energy storage," *Solar Energy Materials and Solar Cells*, vol. 107, pp. 20–27, 2012, doi: 10.1016/j.solmat.2012.07.020.

[7] N. Nallusamy, S. Sampath, and R. Velraj, "Experimental investigation on a combined sensible and latent heat storage system integrated with constant/varying (solar) heat sources," *Renew. Energy*, vol. 32, no. 7, pp. 1206–1227, 2007, doi: 10.1016/j.renene.2006.04.015.

[8] N. Alipour, B. Jafari, and K. Hosseinzadeh, "Analysis of the impact of metal foam with phase change material on solar photovoltaic thermal system efficiency," *Journal of Energy Storage*, vol. 98, Art. no. 113064, 2024, doi: 10.1016/j.est.2024.113064.

[9] H. Li, C. Hu, Y. He, D. Tang, K. Wang, and X. Hu, "Visualized-experimental investigation on the energy storage performance of PCM infiltrated in metal foam with varying pore densities," *Energy*, vol. 237, Art. no. 121540, 2021, doi: 10.1016/j.energy.2021.121540.

[10] H. A. Ahmadi, N. Variji, A. Kaabinejadian, M. Moghimi, and M. Siavashi, "Optimal design and sensitivity analysis of energy storage for concentrated solar power plants using phase change material by gradient metal foams," *Journal of Energy Storage*, vol. 35, Art. no. 102233, 2021, doi: 10.1016/j.est.2021.102233.

[11] N. Prasanth, M. Sharma, R. N. Yadav, and P. Jain, "Designing of latent heat thermal energy storage systems using metal porous structures for storing solar energy," *Journal of Energy Storage*, vol. 32, Art. no. 101990, 2020, doi: 10.1016/j.est.2020.101990.

[12] A. Parida, A. Bhattacharya, and P. Rath, "Effect of convection on melting characteristics of phase change material-metal foam composite thermal energy storage system," *Journal of Energy Storage*, vol. 32, Art. no. 101804, 2020, doi: 10.1016/j.est.2020.101804.

[13] C. Nie, J. Liu, and S. Deng, "Effect of geometry modification on the thermal response of composite metal foam/phase change material for thermal energy storage," *International Journal of Heat and Mass Transfer*, vol. 165, Art. no. 120652, 2021, doi: 10.1016/j.ijheatmasstransfer.2020.120652.

[14] A. R. Karimi, M. Siavashi, M. Tahmasbi, and A. M. Norouzi, "Experimental analysis to improve charge/discharge of thermal energy storage in phase change materials using helical coil and porous metal foam," *Journal of Energy Storage*, vol. 55, Art. no. 105759, 2022, doi: 10.1016/j.est.2022.105759.

[15] M. Ghalambaz, M. Fteiti, O. Younis, M. Sheremet, and H. A. Hasan, "An improved latent heat thermal energy storage using two layers of metal foams," *Appl. Therm. Eng.*, vol. 234, p. 121319, 2023, doi: 10.1016/j.applthermaleng.2023.121319.

[16] S. Liu, H. Wang, Q. Ying, and L. Guo, "Numerical study on the combined application of multiple phase change materials and gradient metal foam in thermal energy storage device," *Appl. Therm. Eng.*, vol. 257, p. 124267, 2024, doi: 10.1016/j.applthermaleng.2024.124267.

[17] V. Joshi and M. K. Rathod, "Experimental and numerical assessments of thermal transport in fins and metal foam infused latent heat thermal energy storage systems: A comparative evaluation," *Appl. Therm. Eng.*, vol. 178, p. 115518, 2020, doi: 10.1016/j.applthermaleng.2020.115518.

[18] Z. Haddad, F. Iachachene, M. A. Sheremet, and E. Abu-Nada, "Numerical investigation and optimization of melting performance for thermal energy storage system partially filled with metal foam layer: New design configurations," *Appl. Therm. Eng.*, vol. 223, p. 119809, 2023, doi: 10.1016/j.applthermaleng.2022.119809.

[19] S. A. M. Mehryan, K. A. Ayoubloo, M. Mahdavi, O. Younis, Z. Kazemi, M. Ghodrat, and M. Ghalambaz, "Optimum configuration of a metal foam layer for a fast thermal charging energy storage unit: A numerical study," *J. Energy Storage*, vol. 48, p. 103950, 2022, doi: 10.1016/j.est.2021.103950.

[20] A. Chibani, S. Merouani, and F. Benmoussa, "Computational analysis of the melting process of phase change material–metal foam-based latent thermal energy storage unit: The heat exchanger configuration," *J. Energy Storage*, vol. 42, p. 103071, 2021, doi: 10.1016/j.est.2021.103071.

[21] R. M. K. Ali and S. Lafta Ghashim, "Numerical analysis of the heat transfer enhancement by using metal foam," *Case Stud. Therm. Eng.*, vol. 49, p. 103336, 2023, doi: 10.1016/j.csite.2023.103336.

[22] A. Arshad, M. Jabbal, H. Faraji, P. Talebizadehsardari, M. A. Bashir, and Y. Yan, "Thermal performance of a phase change material-based heat sink in presence of nanoparticles and metal-foam to enhance cooling performance of electronics," *J. Energy Storage*, vol. 48, p. 103882, 2022, doi: 10.1016/j.est.2021.103882.

[23] M. Valizade, M. M. Heyhat, and M. Maerefat, "Experimental study of the thermal behavior of direct absorption parabolic trough collector by applying copper metal foam as volumetric solar absorption," *Renew. Energy*, vol. 145, pp. 261–269, 2020, doi: 10.1016/j.renene.2019.05.112.

[24] A. D. Brent, V. R. Voller, and K. J. Reid, "Enthalpy-porosity technique for modeling convection-diffusion phase change: Application to the melting of a pure metal," *Numer. Heat Transf.*, vol. 13, no. 3, pp. 297–318, 1988, doi: 10.1080/10407788808913615.

[25] K. Vafai and S. J. Kim, "On the limitations of the Brinkman–Forchheimer-extended Darcy equation," *Int. J. Heat Fluid Flow*, vol. 16, no. 1, pp. 11–15, 1995, doi: 10.1016/0142-727X(94)00002-T.

[26] S. Pati, A. Borah, M. P. Boruah, and P. R. Randive, "Critical review on local thermal equilibrium and local thermal non-equilibrium approaches for the analysis of forced convective flow through porous media," *Int. Commun. Heat Mass Transf.*, vol. 132, p. 105889, 2022, doi: 10.1016/j.icheatmasstransfer.2022.105889.

[27] Q. Ying, H. Wang, and E. Lichtfouse, "Numerical simulation on thermal behavior of partially filled metal foam composite phase change materials," *Appl. Therm. Eng.*, vol. 229, p. 120573, 2023, doi: 10.1016/j.applthermaleng.2023.120573.

[28] T. Bouzennada, A. Abderrahmane, O. Younis, M. Oreijah, K. Guedri, C. Maatki, and L. Kolsi, "Numerical simulation of heat transfer and melting process in a NEPCM: Using new fin shape," *Int. Commun. Heat Mass Transf.*, vol. 143, p. 106711, 2023, doi: 10.1016/J.ICHEATMASSTRANSFER.2023.106711.

[29] ANSYS Inc., *ANSYS FLUENT Theory Guide*, Canonsburg, PA, USA: ANSYS Inc., 2011, p. 794.

[30] S. Huang, J. Lu, and Y. Li, "Numerical study on the influence of inclination angle on the melting behaviour of metal foam-PCM latent heat storage units," *Energy*, vol. 239, p. 122489, 2022, doi: 10.101/10.1016/J.ENERGY.2021.122489.

[31] N. S. Dhaidan and A. F. Khalaf, "Experimental evaluation of the melting behaviours of paraffin within a hemicylindrical storage cell," *Int. Commun. Heat Mass Transf.*, vol. 111, p. 104476, 2020, doi: 10.1016/j.icheatmasstransfer.2020.104476.

[32] C. Ji, Z. Qin, S. Dubey, F. H. Choo, and F. Duan, "Simulation on PCM melting enhancement with double-fin length arrangements in a rectangular enclosure induced by natural convection," *Int. J. Heat Mass Transf.*, vol. 127, pp. 255–265, 2018, doi: 10.1016/j.ijheatmasstransfer.2018.07.118.

[33] N. S. Bondareva and M. A. Sheremet, "Numerical simulation of heat transfer performance in an enclosure filled with a metal foam and nano-enhanced phase change material," *Energy*, vol. 296, p. 131123, 2024, doi: 10.1016/j.energy.2024.131123.